Role of Spin-Orbit Coupling in High-Order Harmonic Generation Revealed by Supercycle Rydberg Trajectories

N. Mayer,[1] S. Beaulieu,[2] Á. Jiménez-Galán,[1,3] S. Patchkovskii,[1] O. Kornilov,[1] D. Descamps,[2] S. Petit,[2] O. Smirnova,[1] Y. Mairesse,[2] and M. Y. Ivanov[1,4,5]

[1]*Max-Born-Institute, Max-Born Straße 2A, 12489 Berlin, Germany*
[2]*Université de Bordeaux—CNRS—CEA, Centre Lasers Intenses et Applications (CELIA), UMR5107, F33405 Talence, France*
[3]*Joint Attosecond Science Laboratory, National Research Council of Canada and University of Ottawa, Ottawa, Canada*
[4]*Department of Physics, Humboldt University, Newtonstraße 15, D-12489 Berlin, Germany*
[5]*Blackett Laboratory, Imperial College London, SW7 2AZ London, United Kingdom*

(Received 7 December 2021; revised 26 July 2022; accepted 8 September 2022; published 18 October 2022)

High-harmonic generation is typically thought of as a sub-laser-cycle process, with the electron's excursion in the continuum lasting a fraction of the optical cycle. However, it was recently suggested that long-lived Rydberg states can play a particularly important role in high harmonic generation by atoms driven by the combination of the counterrotating circularly polarized fundamental light field and its second harmonic. Here we report direct experimental evidence of very long and stable Rydberg trajectories contributing to high-harmonic generation in such fields. We track their dynamics inside the laser pulse using the spin-orbit evolution in the ionic core, utilizing the spin-orbit Larmor clock. We confirm their effect on harmonic emission both via microscopic simulations and by showing how this radiation can lead to a well-collimated macroscopic far-field signal. Our observations contrast sharply with the general view that long-lived Rydberg orbits should generate negligible contribution to the macroscopic far-field high harmonic response of the medium.

DOI: 10.1103/PhysRevLett.129.173202

The interaction of the electron's spin with its orbital motion, the spin-orbit coupling (SOC), is important in atoms, molecules, and solids. Excitation of the spin-orbit-split states upon ionization can either induce ultrafast hole dynamics in the ion [1–3], or generate entanglement between the ion and the photoelectron [4], depending on the degree of coherence created upon ionization [1,4–6]. The latter can be fully controlled with modern attosecond technologies [7].

Yet, the role of spin-orbit interaction in high-harmonic generation (HHG), the process lying at the core of attosecond technologies, and the opportunities it presents for time-resolved spectroscopy of systems in strong laser fields, have largely remained unexplored. In the three step picture of HHG [8,9], field-induced tunneling at time t_i is followed by acceleration of the released electron and radiative recombination with the ionic core at t_r. The delay $\tau = t_r - t_i$, during which the hole can evolve, generally lasts only a fraction of the laser cycle, $\tau \sim 1/\omega$, too short [10] for resolving spin-orbit dynamics in typical HHG media, such as argon or neon in which $\tau\Delta_{SO} \ll 1$, unless very long-wavelength drivers are used [10]. Furthermore, even if electron trajectories long enough to resolve the spin-orbit dynamics existed, their large excursion time $\tau \sim 1/\Delta_{SO} \gg 2\pi/\omega$ is believed to induce extremely large spatiospectral spreading of the macroscopic HHG signal, preventing its observation.

Here we use the built-in Larmor clock offered by spin-orbit interaction [11] to identify both the surprisingly prominent contribution of long-lived Rydberg orbits to the macroscopic HHG signal and the physics responsible for their appearance. Our Letter also confirms the results proposed in [12] that Rydberg states lead to the generation of symmetry-forbidden harmonics.

We study HHG in argon, where coherent excitation of the spin-orbit-split doublet of the $P_{3/2}$ and $P_{1/2}$ core states (splitting $\Delta_{SO} = 0.177$ eV) leads to the precession of the spin of the hole with a period $T_{SO} = 23.5$ fs. If the tunneled electron returns to the core when the hole spin is flipped, recombination is quantum-mechanically prohibited. As a result, the photorecombination amplitude is temporally modulated by the factor $1 + \exp(-i\Delta_{SO}\tau)$. If τ spans at least $\tau \simeq T_{SO}$, this temporal modulation of the emission will spectrally split the harmonic lines by Δ_{SO}. In contrast, if the recombination events contributing to HHG occur within a fraction of the laser cycle with $\omega \gg \Delta_{SO}$, no spin-orbit splitting will be seen [10]. Experimentally, we observe well-collimated high harmonic emission split by Δ_{SO} in Ar driven by circularly polarized 800 nm fundamental field and its counterrotating second harmonic. Our results show that this splitting can only occur due to long-lived electron orbits lasting at least $T_{SO} \simeq 23.5$ fs. It allows us to show how multiphoton Freeman resonances [13,14] shape the

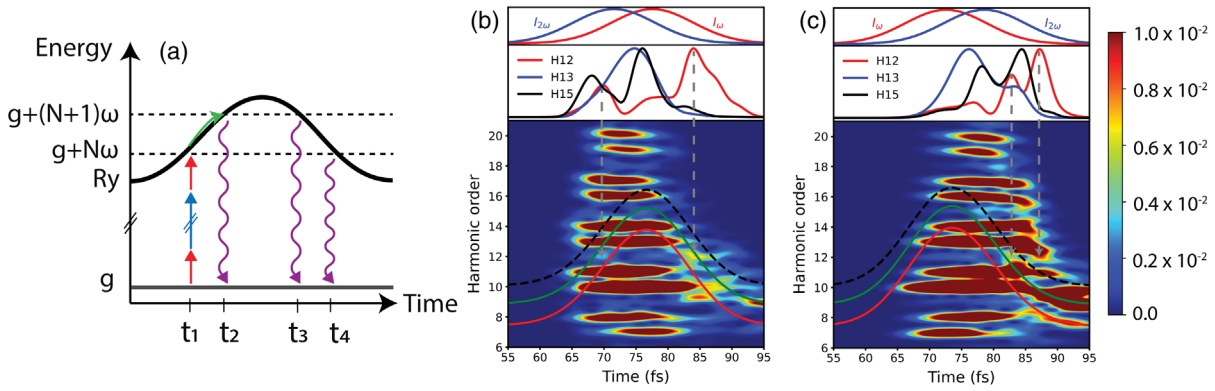

FIG. 1. The role of the Rydberg state in multicycle bicircular HHG. (a) Resonant multiphoton transitions to Stark-shifted Rydberg states can occur at the rising (t_1) or falling edges (t_4) or near the pulse peak (t_2, t_3) (see text for details). (b),(c) Calculated Gabor spectrogram (Gaussian window of FWHM $= 2\pi/\omega$) of the harmonic emission obtained by solving the TDSE in argon. The time-dependent energy of the ponderomotive-shifted ionization potential (dashed black line), $2p^5 3d$ state (green solid line) and $2p^5 4s$ state (red solid line) are also shown. Inset [(b) and (c)]: Time-dependent emission of selected harmonics, i.e., symmetry-allowed H13 and forbidden H12 and H15. The intensity envelope of the two pulses are shown in the topmost panel. In (b) the 2ω field precedes the ω field ($\tau = 6$ fs), vice versa in (c) ($\tau = -6$ fs). Both fields have an ellipticity of $\epsilon = 0.9$.

harmonic emission in time and space, and how their contribution emerges in the far field.

Figure 1(a) shows how resonantly populated Rydberg states participate in the HHG process at the single atom level [15,16]. They are populated through light-induced Freeman resonances [13,14], the frequency-domain counterpart of the time-domain frustrated tunneling [17]. Resonances can arise on the rising and falling edges of the pulse, or near its peak [times t_i of Fig. 1(a)], when

$$E_n + U_p(t) - E_g = n_\omega \omega + n_{2\omega} 2\omega, \tag{1}$$

where $n_{r\omega}$ is the number of absorbed photons from the $r\omega$ field, E_n is the field-free energy of the Rydberg state, and the ac Stark shift is approximated by the ponderomotive energy $U_p(t) = U_p^{\omega}(t) + U_p^{2\omega}(t)$, with $U_p^{r\omega}(t) = E_{r\omega}^2(t)/2(r\omega)^2$.

Concomitant with resonant excitation at times t_1, resonant emission from Rydberg states can occur, also enhanced by constructive cycle-to-cycle interference. Indeed, for a Rydberg orbit, the relative phase ϕ accumulated between the two successive emission events separated by the optical cycle $T_{\rm cyc}$ is $\phi = (E_n + U_p - E_g)T_{\rm cyc}$. Their constructive interference requires $\phi = (E_n + U_p - E_g)T_{\rm cyc} = 2\pi m$, i.e., $E_n + U_p - E_g = m\omega$, optimizing emission from the Rydberg states at integer harmonic orders and on resonance with the ground state.

Importantly, Rydberg excitations can lead to the emission of symmetry-forbidden (e.g., parity forbidden) harmonics, which in the specific case of bicircular $(\omega, 2\omega)$ fields are harmonics with order $3N$ [12]. Let excitation on the rising edge [time t_1 in Fig. 1(a)] populate a Rydberg state that can recombine via a dipole transition to the ground state. After excitation, the excited Rydberg state is shifted up in energy [green line in Fig. 1(a)]. At a later time [t_2 or t_3 in Fig. 1(a)], the Rydberg state again enters a multiphoton resonance with the ground state. Even if the resonant energy formally corresponds to symmetry-forbidden harmonic lines, radiative recombination can occur without violating conservation rules since the parity and the angular momentum of the Rydberg state is conserved by the ponderomotive shift. Forbidden harmonic generation is thus an evidence of a supercycle Rydberg trajectory that starts at a resonant time t_1 and recombines later at a resonant time t_2. The combination of the cycle-to-cycle interference and the ponderomotive shift of the Rydberg state thus effectively act as a temporal gate on the dipole moment $\mathbf{d}(t)$, enhancing the harmonic emission near the resonant times t_i, at both allowed and forbidden frequencies.

To support this picture we have performed TDSE simulations in Ar using the code of Patchkovskii *et al.* [18]. We use a bicircular field composed of two Gaussian pulses centered at 800 and 400 nm, both of 15 fs FWHM duration, with peak intensities of $I_\omega = I_{2\omega} = 7 \times 10^{13}$ W/cm^2. To account for experimental polarization state artifacts, we consider pulses with ellipticity $\epsilon_\omega = \epsilon_{2\omega} = 0.9$ (calculations for circularly polarized light $\epsilon_\omega = \epsilon_{2\omega} = 1.0$ show no qualitative differences). At the peak of the pulse, the total ponderomotive shift is $U_p \simeq 7\omega$. Figures 1(b) and 1(c) show the Gabor spectrogram of the dipole acceleration $\ddot{\mathbf{d}}(t)$ obtained using a Gaussian window function with FWHM of one optical cycle $T_{\rm cyc} = 2\pi/\omega$. As shown in Ref. [12], harmonic generation from Rydberg states is enhanced in a bicircular pulse when the pulses are not overlapping and when the 2ω pulse precedes the ω one. We thus construct a time-frequency spectrogram (the Gabor spectrogram) of the harmonic emission for two relative delays: $\tau = 6$ fs in Fig. 1(b) where 2ω precedes ω, and $\tau = -6$ fs in Fig. 1(c), when ω precedes 2ω one.

The dashed black line shows the ponderomotive shift of the ionization potential, while the solid red and green lines show the ponderomotive shift of the Rydberg states $2p^5 4s$ and $2p^5 3d$, respectively. The top panel shows the time-dependent emission for H12, H13, and H15, obtained by integrating the Gabor spectrogram around the corresponding energies, in the $\pm 0.25\omega$ range. For both forbidden harmonics H12 and H15 the contribution of Rydberg states is more visible than for the allowed H13, where short trajectories dominate the emission. Because of imperfect circularity of the pulses, absorption of counter-rotating components from either field can now lead to 3N harmonic orders. Nonetheless, resonant enhancement of these orders is clearly observed in Figs. 1(b) and 1(c).

When the second harmonic precedes the fundamental pulse [Fig. 1(b)], enhanced emission of both H12 and H15 is observed near -7 fs. At this time, the Rydberg states just below the ionization threshold, and the $2p^5 4s$ state enter resonance with the two adjacent harmonics. In agreement with Fig. 1(a), we interpret the enhancement as a signature of Rydberg states excited by a multiphoton resonance that can later recombine at a "forbidden" harmonic. Similarly at around 0 fs, enhancement of H12 and H15 is due to the multiphoton resonance of the $2p^5 3d$ state at the H15 energy. On the falling edge ($\sim$7 fs) the H12 is enhanced again due to the resonance with the $2p^5 3d$ state.

When the fundamental pulse precedes its second harmonic [Fig. 1(c)], the shape of the temporal gate changes drastically: resonant enhancements are seen mainly on the falling edge. In agreement with Refs. [12,19], this change reflects the reduction (when compared to the case of 2ω preceding ω) in the associated very long trajectories. The time the trapped Rydberg population spends inside the pulse is thus longer when the 2ω field precedes the ω one (positive delays).

We now take advantage of this temporal gating of the HHG emission to resolve the spin-orbit hole dynamics in the core. The well-defined start of the spin-orbit clock is provided by the light-induced multiphoton resonance: the time window during which the ponderomotive shift brings a Rydberg state into a multiphoton resonance with the ground state is much shorter than the pulse duration. Upon excitation, the emission from the Rydberg state is modulated in time with the spin-orbit period, leading to the splitting of the harmonic lines by Δ_{SO} (see Fig. 2). The appearance of the splitting is the evidence of the long-lived Rydberg orbits. As noted above, the time spent by the trapped Rydberg orbits during the pulse is substantially longer when 2ω precedes the ω: this is where the spin-orbit splitting is expected to appear.

We performed experiments in argon, with $\Delta_{SO} = 0.177$ eV corresponding to $T_{SO} = 23.5$ fs, using the setup described in the Supplemental Material [20]. Figure 3(a) shows the ratio between selected forbidden and allowed harmonic orders as a function of the relative time delay,

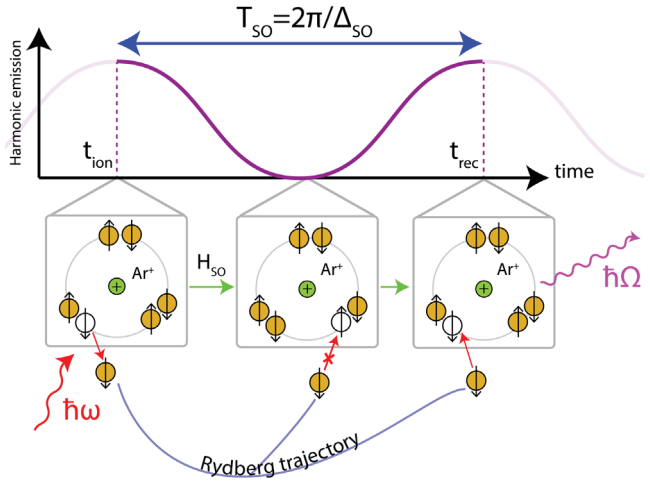

FIG. 2. Spin-orbit temporal modulation of the emission leading to spectral splitting of the harmonic lines. Radiative electron-hole recombination is temporally modulated due to the precession of the spin of the hole, leading to a spectral splitting of the harmonic lines.

where for positive time delays the 2ω field precedes the ω one. The delay dependence of the forbidden harmonics confirms the behaviour predicted in [12] and our TDSE simulations: the participation of Rydberg states in HHG is optimized when 2ω precedes ω. Figure 3(b) shows the far-field spatially resolved harmonic spectrum at positive and negative delays. At positive delays we see strong enhancement of forbidden 3N orders due to Rydberg states. Moreover, we observe spectral splitting of most harmonic lines, consistent with the spin-orbit energy of argon. The thin gas jet used in the experiment excludes longitudinal phase matching and propagation effects. Therefore we conclude that, by trapping the Rydberg electron for $\sim$24 fs at intensities of $I \sim 2 \times 10^{14}$ W/cm^2, we resolve the spin precession of the electron hole in the core. The absence of the spectral splitting at negative time delays is consistent with the discussion above: when ω precedes 2ω, trapping occurs at the falling edge of the pulse, leaving insufficient time to resolve the spin-orbit-induced modulation.

Thus, our experiment shows collimated far-field contribution of trajectories spending ten (or more) cycles in the Rydberg states. However, such trajectories should accumulate a large intensity-dependent phase (see, e.g., Refs. [21–23].) Because of spatiotemporal intensity distribution in the focal region, one would therefore expect large spectral broadening and large divergence of the corresponding signal. Yet, we see a collimated harmonic signal in the far field. How is that possible? Our explanation is associated with the resonant nature of the process, which selects a specific spatial region in the laser focus, where the resonance(s) with Stark-shifted Rydberg state(s) is achieved. The intensity of the driving field is approximately constant along this ring. There, the resonant contribution to the harmonic emission is maximally enhanced, and,

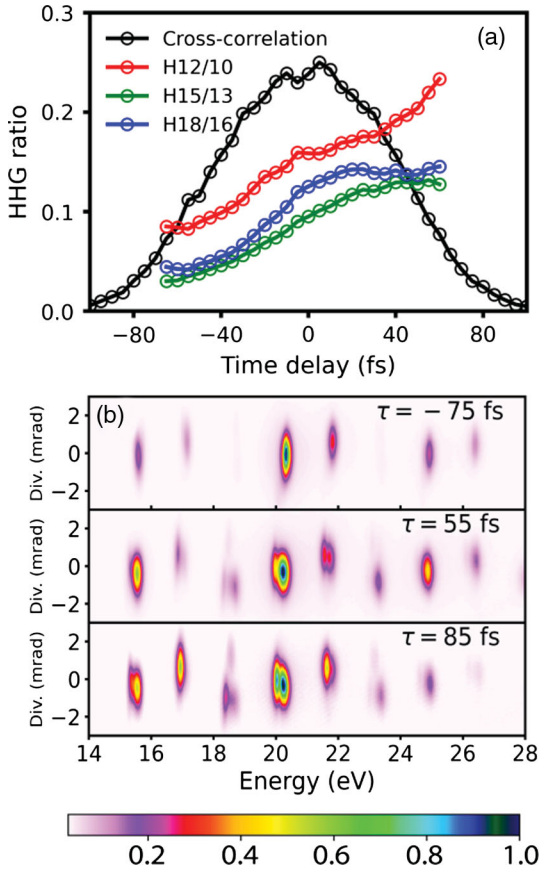

FIG. 3. Experimental results. (a) Measured delay-dependent total harmonic yield (black) and ratio between $3N$ and $3N-2$ harmonics: H12/H10 (red), H15/13 (green), H18/16 (blue). (b) Far-field HHG spectrum with ω field preceding ($\tau = -75$ fs) or following ($\tau = 55$ fs, 85 fs) the 2ω field. For $\tau = 55$, 85 fs, enhanced generation of forbidden harmonics and spin-orbit splitting of most harmonics are observed.

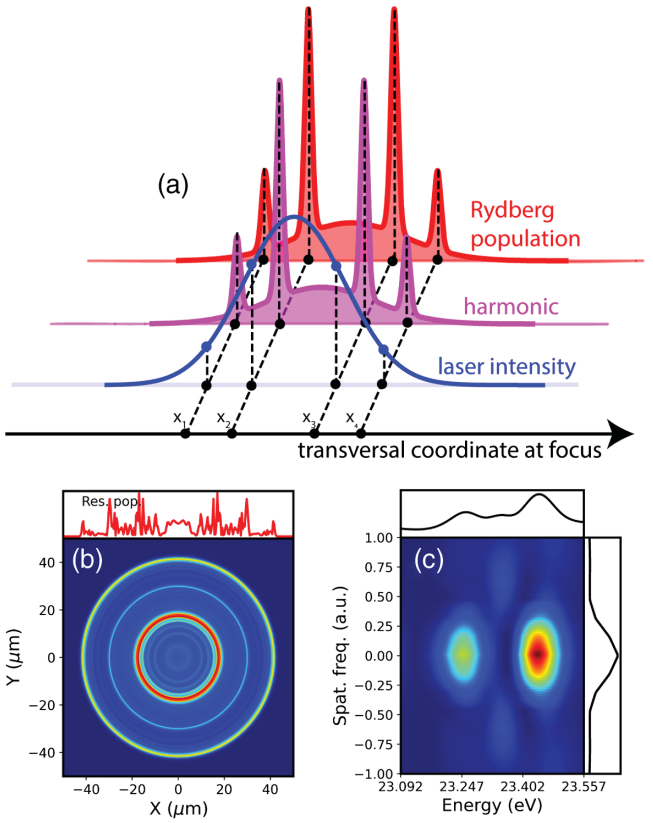

FIG. 4. The role of spatiotemporal gating in the generation of collimated spin-orbit split harmonics. (a) Spatial gating: multiphoton resonances with Stark-shifted Rydberg states lead to resonant enhancements of a given harmonic at positions $\mathbf{x}_i$, defining onion shells where the harmonic phase is large but constant. (b),(c) Results from the two-level system model; (b) the near-field profile of H15, (c) the spin-orbit splitting of H15 in the far field. The top panel in (b) shows the spatial distribution of the residual population in the excited state at the end of the pulse. The top panel in (c) shows the frequency-resolved, spatially integrated distribution in the far field of H15 when spin-orbit modulations are included, while the right panel in (c) shows the frequency-integrated, spatially resolved far-field H15 line.

moreover, the phase of the emission is fixed, leading to a collimated far-field pattern. The same spatial region provides the dominant contribution to Freeman resonances in photoelectron spectra [14,24]. Thus, resonances with Rydberg states provide an addition spatial gating to the harmonic emission, see Fig. 4(a), complementary to the time-domain gating explained earlier.

To confirm this picture, we model high-harmonic generation from an excited state using the two-level system (TLS) described in the Supplemental Material [20]. The TLS includes the ground and pondermotively shifted excited state. To mimick the spin-orbit modulations, we multiply the obtained dipole moment by the oscillating term $[1+\exp(-i\Delta_{\mathrm{SO}}t)]$, where $\Delta_{\mathrm{SO}} = 0.007$ a.u. is the spin-orbit energy. The near-field profile of H15 [Fig. 4(b)] shows resonant enhancements when the multiphoton resonance is reached near the peak of the field. The residual population of the excited state, shown above the near-field profile in red, peaks at the same positions. In the far field, Fig. 4(c), we observe a well-collimated, spin-orbit-split harmonic line.

Our Letter sheds new light on the role of Rydberg states in the HHG process. The influence of excited states in HHG has been the subject of many experimental [15,25–28] and theoretical studies [29–31]. On very short timescales, Rydberg excitations followed by ionization and recombination into the ground state lead to a delayed (by a few femtoseconds) emission of an attosecond pulse train [15]. On longer timescales, the population of Rydberg states can induce hyper-Raman lines [27,32] if a dressing laser field is added. On the timescales much longer than the laser pulse duration, a Rydberg wave packet generates coherent XUV free-induction decay (FID) [26,33]. Here we work in an intermediate range, where we demonstrate the coherent emission of XUV radiation through strong-field driven electron trajectories lasting several tens of femtoseconds. The identified mechanism provides a link between the

Freeman resonances and the HHG process [13,29,34]. Our Letter shows that the spin-orbit Larmor clock allows one to monitor the presence of Rydberg orbits living at least ~24 fs inside a laser pulse with intensities of 200 TW/cm^2, opening the perspective of probing the dynamics of electronic wave packets over tens of femtoseconds by extending HHG spectroscopy beyond the optical cycle.

N. M. and M. I. acknowledge support from DFG QUTIF: IV 152/6-2. Á. J-G. acknowledges support from the H2020 Marie Skłodowska-Curie Actions (101028938). This project has received funding from the European Research Council (ERC) under the European Unions Horizon 2020 research and innovation Program No. 682978 - EXCITERS, and from the French National Research Agency through ANR-14-CE32-0014 MISFITS.

[1] E. Goulielmakis, Z.-H. Loh, A. Wirth, R. Santra, N. Rohringer, V. S. Yakovlev, S. Zherebtsov, T. Pfeifer, A. M. Azzeer, M. F. Kling, S. R. Leone, and F. Krausz, Nature (London) **466**, 739 (2010).
[2] M. Kübel, Z. Dube, A. Y. Naumov, D. M. Villeneuve, P. B. Corkum, and A. Staudte, Nat. Commun. **10**, 1042 (2019).
[3] Y. Kobayashi, K. F. Chang, S. M. Poullain, V. Scutelnic, T. Zeng, D. M. Neumark, and S. R. Leone, Phys. Rev. A **101**, 063414 (2020).
[4] O. Smirnova, Nature (London) **466**, 701 (2010).
[5] S. Pabst, M. Lein, and H. J. Wörner, Phys. Rev. A **93**, 023412 (2016).
[6] M. Ruberti, Phys. Chem. Chem. Phys. **21**, 17584 (2019).
[7] M. J. J. Vrakking, Phys. Rev. Lett. **126**, 113203 (2021).
[8] M. Lewenstein, P. Balcou, M. Y. Ivanov, A. L'Huillier, and P. B. Corkum, Phys. Rev. A **49**, 2117 (1994).
[9] P. B. Corkum, Phys. Rev. Lett. **71**, 1994 (1993).
[10] S. Pabst and R. Santra, J. Phys. B **47** (2014).
[11] J. Kaushal, F. Morales, L. Torlina, M. Ivanov, and O. Smirnova, J. Phys. B **48**, 234002 (2015).
[12] A. Jiménez-Galán, N. Zhavoronkov, M. Schloz, F. Morales, and M. Ivanov, Opt. Express **25**, 22880 (2017).
[13] R. R. Freeman, P. H. Bucksbaum, H. Milchberg, S. Darack, D. Schumacher, and M. E. Geusic, Phys. Rev. Lett. **59**, 1092 (1987).
[14] G. N. Gibson, R. R. Freeman, T. J. McIlrath, and H. G. Muller, Phys. Rev. A **49**, 3870 (1994).
[15] S. Beaulieu, S. Camp, D. Descamps, A. Comby, V. Wanie, S. Petit, F. Légaré, K. J. Schafer, M. B. Gaarde, F. Catoire, and Y. Mairesse, Phys. Rev. Lett. **117**, 203001 (2016).
[16] S. Camp, S. Beaulieu, K. J. Schafer, and M. B. Gaarde, J. Phys. B **51**, 064001 (2018).
[17] H. Zimmermann, S. Patchkovskii, M. Ivanov, and U. Eichmann, Phys. Rev. Lett. **118**, 013003 (2017).
[18] S. Patchkovskii and H. Muller, Comput. Phys. Commun. **199**, 153 (2016).
[19] M. V. Frolov, N. L. Manakov, A. A. Minina, A. A. Silaev, N. V. Vvedenskii, M. Y. Ivanov, and A. F. Starace, Phys. Rev. A **99**, 053403 (2019).
[20] See Supplemental Material at http://link.aps.org/supplemental/10.1103/PhysRevLett.129.173202 for a detailed description of the experimental setup and the two-level system used to simulate the far-field macroscopic response.
[21] P. Salières, A. L'Huillier, and M. Lewenstein, Phys. Rev. Lett. **74**, 3776 (1995).
[22] M. B. Gaarde and K. J. Schafer, Phys. Rev. A **65**, 031406(R) (2002).
[23] F. Catoire, A. Ferré, O. Hort, A. Dubrouil, L. Quintard, D. Descamps, S. Petit, F. Burgy, E. Mével, Y. Mairesse, and E. Constant, Phys. Rev. A **94**, 063401 (2016).
[24] P. Agostini and L. F. DiMauro, Phys. Rev. A **47**, R4573 (1993).
[25] M. Chini, X. Wang, Y. Cheng, H. Wang, Y. Wu, E. Cunningham, P.-C. Li, J. Heslar, D. A. Telnov, S.-I. Chu, and Z. Chang, Nat. Photonics **8**, 437 (2014).
[26] S. Beaulieu, E. Bloch, L. Barreau, A. Comby, D. Descamps, R. Géneaux, F. Légaré, S. Petit, and Y. Mairesse, Phys. Rev. A **95**, 041401(R) (2017).
[27] E. Bloch, S. Beaulieu, D. Descamps, S. Petit, F. Légaré, A. Magunov, Y. Mairesse, and V. Strelkov, New J. Phys. **21**, 073006 (2019).
[28] H. Yun, J. H. Mun, S. I. Hwang, S. B. Park, I. A. Ivanov, C. H. Nam, and K. T. Kim, Nat. Photonics **12**, 620 (2018).
[29] R. Taïeb, V. Véniard, J. Wassaf, and A. Maquet, Phys. Rev. A **68**, 033403 (2003).
[30] X.-B. Bian and A. D. Bandrauk, Phys. Rev. Lett. **105**, 093903 (2010).
[31] S. Camp, K. J. Schafer, and M. B. Gaarde, Phys. Rev. A **92**, 013404 (2015).
[32] T. Millack and A. Maquet, J. Mod. Opt. **40**, 2161 (1993).
[33] S. Bengtsson, E. W. Larsen, D. Kroon, S. Camp, M. Miranda, C. L. Arnold, A. L'Huillier, K. J. Schafer, M. B. Gaarde, L. Rippe, and J. Mauritsson, Nat. Photonics **11**, 252 (2017).
[34] J. Wassaf, V. Véniard, R. Taïeb, and A. Maquet, Phys. Rev. A **67**, 053405 (2003).